

## Finite element analysis of fibre-reinforced constitutive formulation of Cadisc-L

**Ali Ansari<sup>a</sup>, Hamidreza Ghasemi Bahraseman<sup>b\*</sup>, Morteza Mohssenzadeh<sup>c</sup>, Mohammad Haghpanahi<sup>a</sup>, Kamran Hassani<sup>a</sup> and Hossein Derakhshandeh<sup>d</sup>**

<sup>a</sup>Department of Biomechanics, Science and Research Branch, Islamic Azad University, Tehran, Iran

<sup>b</sup>Mechanical Engineering Department, San Diego State University, San Diego, 92182, CA, USA

<sup>c</sup>Mechanical Engineering Department, University of San Diego, San Diego, 92110, CA, USA

<sup>d</sup>Department of Mechanical & Material Engineering, University of Nebraska-Lincoln, Lincoln, NE 68588, USA

### ARTICLE INFO

#### Article history:

Received 10 October, 2018

Accepted 24 December 2018

Available online

24 December 2018

#### Keywords:

Cadisc-L

Finite element method

Fibre-reinforced constitutive

formulation

### ABSTRACT

The current study measures the mechanical behavior of both natural and the monobloc elastomeric disc prosthesis (Cadisc™-L) by employing a finite element method (FEM) to study the fiber-reinforced constitutive formulation provided in the literature. The three-dimensional geometry was created by computed tomography (CT) scan imaging technique. Frontal pure rotational, sagittal, and axial momentum of 7.5 N·m were applied on the top of L3 while the lower half of the L5 was fixed in all directions. This investigation was performed considering two stages: (1) intact L3–L5 lumbar spine (INT model), and (2) Cadisc implemented between L4 and L5 (IMP model). The numerical results for the INT model were validated by experimental data from the literature. Several parameters including the inter-segmental rotation, range of motion in flexion-extension, axial rotation and lateral bending were analyzed. Our numerical results show that the IMP model has a 50% reduction in the ‘range of motion’ and a 33% reduction in flexion in lateral bending compared to the INT model. These outcomes of this paper reveal the feasibility of applying a fibre-reinforced constitutive formulation to generate an accurate three-dimensional FEM model.

© 2019 Growing Science Ltd. All rights reserved.

## 1. Introduction

Despite progresses in prevention, diagnosis, and treatment of intervertebral disc problems, such problems remain a main cause of disability for humans (Joshi et al., 2006). Elderly people, after the appearance of instability in their spinal column, may suffer from pain due to the degeneration of intervertebral discs and they usually need implantation with an artificial disc (Dietrich et al., 2005). Discovering the effect of geometry and tissue properties is challenging in the numerical modeling approaches due to the high intrinsic parameters existing in the experiment (Berkson et al., 1979; Nachemson et al., 1979; Skultz et al., 1979). Furthermore, a major limitation of in-vitro explorations is quantification of load transfer between different tissues that are constrained by range of motion including global reaction forces and intradiscal pressure. Computational methods, however, have the potential to determine the biomechanical behavior of natural and artificial intervertebral discs by eliminating the need for experimental procedures provided that their procedures meet validation criteria.

\* Corresponding author. Tel.: +1-901-567-8750  
E-mail addresses: [hghasemibahraseman@sdsu.edu](mailto:hghasemibahraseman@sdsu.edu) (H. Ghasemi Bahraseman)

The finite element method is widely used for strain and stress analysis of engineering structures particularly in biomechanics and proved to be very functional for complex models of living tissues structures (Amerian et al., 2014; Bahraseman et al., 2013, 2014a, 2014b, 2015 & 2016; Dietrich et al., 1991; Kedzior et al., 1996; Khosravi et al., 2014a & 2014b; Poor et al., 2017; Sabooni et al., 2015; Skalli, 1999; Zienkiewicz & Taylor, 1991). These computational tools provide assistance for a better interpretation of clinical and experimental data to improve the prosthesis design. The Cadisc-L is produced from a polyurethane-polycarbonate polymer using stiff endplates. The internal structure of Cadisc-L consists of a soft nucleus encircled by a stiffer annulus that is segregated by a gradual transition of modulus (Naylor et al., 2012; Gwynne et al., 2010; Gwynne & Cameron, 2010; Barnes et al., 2012).

The advantage of having separated regions is to eliminate sharp interfaces among materials with different mechanical properties (Gwynne & Cameron, 2010). The design of the implant nearly imitates the mechanical properties of the natural disc (Naylor et al., 2012; Gwynne et al., 2010; Johnson et al., 2011; Benzel et al., 2011). Langrana et al. (1991) performed a finite element analysis approach to model an ideal and a realistic disc. They studied the mechanical behavior of such discs with varying extends and types of injuries and degenerations by considering the effects of geometry, the relative volumes of the nucleus to annulus fibrosus, the fiber volume fraction and material properties. Gloria et al. (2011) investigated the static and dynamic mechanical properties of an in-house developed composite IVD prostheses. The composite IVD was made out of reinforced poly semi-interpenetrating polymer network hydrogel with the same structure as the natural IVD using filament winding and molding techniques. Their findings revealed appropriate static and dynamic mechanical characteristics that was similar to natural IVD. Later in 2012, Noailly et al. (2012) performed a numerical simulation on annulus fibrosus (AF) repair. Their study investigated the performance of a tested biomimetic composite disc implant made of an artificial polymer nucleus contained within a fiber-reinforced textile annulus. Their implant design optimization study was aimed to match the natural disc's overall biomechanical properties. Their numerical results showed the importance of fiber orientation on the control of torsional loading. Their techniques emphasized the capabilities and potentials of simulation models to quickly screen repair tactics and design advancement of AF repair means. The rotations with the controlled load and displacement were modeled with respect to the body weight. The equipment updates help rebuilding the model's estimations on global axial and sagittal flexibility. Material properties played a major role, but some other updates were identified to potentially tune the device behavior against specific motions. All device versions altered the coupled intersegmental shear deformations affecting facet joint contact through contact area displacements. Loads in the bony endplates adjacent to the implants increased as the implant stiffness decreased but did not appear to be a strong limitation for the implant biomechanical and mechanobiological functionality. In conclusion, numerical results given by biomimetic composite disc substitutes were encouraging with greater potential than that offered by ball-on-socket implants.

Van den Broek et al. (2012) considered four cases of homogeneous elastomer, elastomer with fiber jacket, multi-stiffness elastomer, and hydrogel with fiber jacket using a computational method where the fiber jacket around an elastomer case considered the physiological motion in all degrees of freedom. They concluded that mimicking the non-linear behavior of intervertebral disk is essential in supporting the spinal motion. Van de Broek et al. (2012) tested in-vitro in axial compression with a unique loading to investigate the strength of a biomimetic artificial intervertebral discs (AID). They revealed a natural disc annulus design that is very comparable to natural disc behavior. There are several investigations on intervertebral discs for healthy and pathologic cases mainly experimentally (Brown et al., 1957; Adams et al., 1980; Tencer et al., 1982; Twomey & Taylor, 1983; Goel et al., 1985; Miller et al., 1986; McNally et al., 2012).

This investigation aims to apply FEM analysis to both natural and artificial intervertebral discs (Cadisc-L embedded between L4, L5) using a fiber-reinforced constitutive formulation (Holzapfel & Stadler, 2006). The numerical simulations were performed for an intact L3–L5 lumbar spine model (INT) as well as the L3-L5 lumbar spine with a Cadisc implemented between L4 and L5 (IMP). The goal of the current study is to analyze the influence of disc implementation on segment mechanics, intersegmental rotation, range of motion, Intradiscal pressure and Intradiscal von-Mises stress.

## 2. Materials and methods

### 2.1 Geometry

The CT scan DICOM file of the L3–L5 lumbar spine of a male aged 27 was acquired at 0.35 mm intervals to make a three-dimensional FE model. The CT dataset was imported into the medical image processing software (Mimics (10.0.0.188), Materialise NV, Belgium) to create a 3-dimensional geometric dataset including point clouds. A modified polygonal set of data was extracted by Geomagic Studio (Research Triangle Park, NC) and the final surface geometry was created by commercially available software CATIA v5R20 (Dassault systems Inc.). The CAD model was imported to the FE analysis software Abaqus 6.12.1 (Simulia, Dassault Systems) to create a 3-dimensional FE model, Fig. 1a. The model is composed of 4 parts; two endplates- PU160 (Fig. 1c) and the two different modulus of bearing body (Fig. 1d).

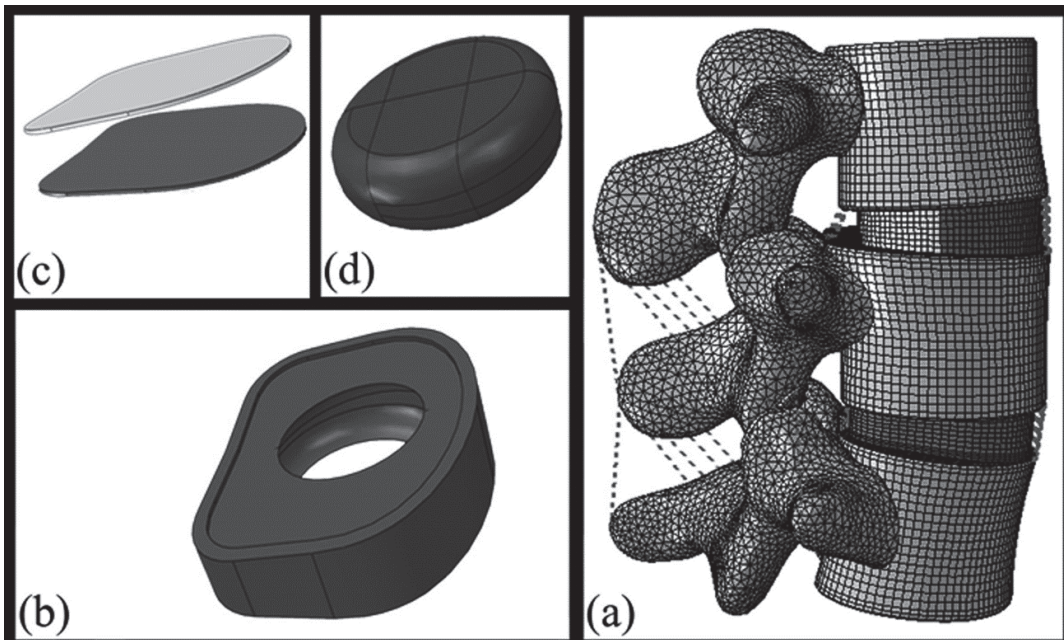


**Fig. 1.** Sagittal view of the L3–L5 lumbar spine bi-segment (a) and Cadisc-L parts including outer part of the bearing body (b), top and bottom endplates (c) and inner part of the bearing body (d).

#### 2.1. FE Model

Two FE models of lumbar spine were developed in this study: An intact lumbar spine (INT) and the implanted Cadisc between L4 and L5 (IMP). The INT model consisted of 181,081 elements and 104,035 nodes. Both models have an osteoligamentous lumbar spine which are comprised of the vertebrae, intervertebral discs, endplates, posterior bony elements, and all seven ligaments, Superspinous (SSL), Interspinous (ISL), Intertransverse (ITL), Capsular (CL), Ligamentum Flavum (LF), Posterior longitudinal (PLL) and anterior longitudinal (ALL). The implant was located at the space between L4-L5 utilizing the assembly tools available in Abaqus CAE. Surfaces were produced at the interface of the implant and the vertebral body, and the interface of the implant parts by defining

an interaction (Tie Constraint). The space between the posterior vertebral elements at the facet joint was also identified and masked to represent the facet joint.

## 2.2 Mechanical Properties

The material properties of the INT model are listed in table 1 and were derived from the literature (Holzapfel & Stadler, 2006; Noailly et al., 2005; Shirazi et al., 1986; Denozi'ere, 2004; Natarajan & Andersson, 1999; Rohlmann et al., 2006; Goel et al., 1995). The material properties of the ligaments are defined as non-linear elastic properties (Shin et al., 2007), and they were arranged in the anatomical direction as reported (Chen et al., 2009). The computational model in this study uses non-compressive loading resistance for ligament.

**Table 1.** Summary of the material properties used for the intact modeling

Material Properties	Nucleus pulposus	Hyperelastic (Mooney–Rivlin): C10=0.12MPa, C01=0.09MPa, D=0.0667 (Noailly et al., 2005)	
	Posterior element	E=3500 MPa, v=0.3 (Shirazi et al., 1986)	
	End Plate	E=12000 MPa v=0.3 (Denozi'ere, 2004)	
Vertebral Body	Cortical: E=12000 MPa, v=0.3; Cancellous: E=100 MPa, v=0.2 (Natarajan & Andersson, 1999)		
Anulus Fibrosus	Ventral	Annulus fibers : k1=2 N/mm, k2=5 N/mm , Fiber Angle = -30 deg30 deg (Holzapfel & Stadler, 2006)	
	Dorsal	Ground substance of annulus : C10=0.348 MPa , D=0.3 MPa (Rohlmann et al, 2006)	
Facet Joints	gap 0.5 mm and frictionless after Contact (Natarajan & Andersson, 1999; Goel et al, 1995)		
Ligaments (Shin et al, 2007)	Ligament	Young's modulus (MPa)	Cross-section (mm <sup>2</sup> )
	Anterior longitudinal ligament (ALL)	7.8 ( $\varepsilon < 12\%$ ), 20 ( $\varepsilon > 12\%$ )	63.7
	Posterior longitudinal ligament (PLL)	1.0 ( $\varepsilon < 11\%$ ), 2.0 ( $\varepsilon > 11\%$ )	20
	Ligamentum flavum (LF)	1.5 ( $\varepsilon < 6.2\%$ ), 1.9 ( $\varepsilon > 6.2\%$ )	40
	Transverse ligament (TL)	10 ( $\varepsilon < 18\%$ ), 59 ( $\varepsilon > 18\%$ )	1.8
	Capsular ligament (CL)	7.5 ( $\varepsilon < 25\%$ ), 33 ( $\varepsilon > 25\%$ )	30
	Interspinous ligament (IL)	25%)	40
	Supraspinous ligament (SL)	1.0 ( $\varepsilon < 14\%$ ), 1.2 ( $\varepsilon > 14\%$ )	30
		3.0 ( $\varepsilon < 20\%$ ), 5.0 ( $\varepsilon > 20\%$ )	

Hexahedron elements (8-noded cubic element) were used in discretizing the governing equations of the model of cortical bone, cancellous bone, endplate, annulus fibrosus, and finally nucleus pulposus. The hexahedron element in three-dimensional finite element modeling has proved to be the most effective element to use in structure mechanical simulation (Logan, 1992). Cortical bone and cancellous bone were assumed to be homogeneous and isotropic (Chen et al., 2009). The nucleus pulposus which lies at the middle of the disc is made of strands of fibre . The annulus fibrosus which surrounds the nucleus pulposus is made up of bands of fibre embedded in the matrix. The annulus fibrosus was simulated by using a hyperelastic, two-parameter Neo-Hookean formulation (Eberlein et al., 2001). A hyper-elastic material was used with a shear modulus representing the ligament and the membrane (Table 2) (Natarajan & Andersson, 1999; Goel et al., 1995). The facet joint was treated as a sliding contact problem applying surface-to-surface contact elements with a coefficient of friction equal to 0.1 (Polikeit et al., 2003; Chen et al., 2001). The beginning gap between a pair of facet surfaces was considered to be 0.5 mm. For the IMP model, Cadisc mechanical properties were derived from the

literature (Falodi, 2010). This was simulated by using a hyperelastic, 2<sup>nd</sup> order Polynomial formulation and was considered incompressible (Falodi, 2010).

**Table 2.** Material properties used for the Cadisc

Material	Nucleus (PU90)	Outer Part of the bearing Body (PU210)	End Plate (PU161)
Hyperelastic polynomial strain energy with N = 2	C <sub>10</sub> = 0.676271134 C <sub>01</sub> = 0.18496083 C <sub>20</sub> = 0.05182980979 C <sub>11</sub> = -0.166393131 C <sub>02</sub> = 0.04545302067	C <sub>10</sub> = 0.879470428 C <sub>01</sub> = 0.198390606 C <sub>20</sub> = 0.066682233 D <sub>1</sub> =0.0 D <sub>2</sub> =0.0 C <sub>11</sub> = -0.193089765 D <sub>2</sub> =0.0 C <sub>02</sub> = 0.0411039155	-
Elastic	-	-	E=1000 $\nu=0.4$
Plastic	-	-	Yield Stress = 30 MPa Plastic Strain= 0.1

### 2.2.1 Strain Energy Potential

The annulus fibrosus of natural disc was modeled as a transversely anisotropic material and assumed to be compressible and defined using the strain-energy function:

$$\Psi(C, A) = \psi_m(\bar{C}) + \psi_f(\bar{C}, A) + L(J), \quad (1)$$

where the first term in the right hand side is the derivative strain energy density of the matrix, Eq. (2)

$$\psi_m = \frac{c}{2}(\bar{I}_1 - 3). \quad (2)$$

The second term of the right hand side of Eq. (1) is the stored energy in the fibers, Eq. (2)

$$\psi_f = \frac{k_1}{2k_2} \left\{ \exp[k_2 (\bar{I} - 1)^2] - 1 \right\}, \quad (3)$$

deviatoric strain energy density of the matrix,

$$L(J) = \frac{\kappa}{2}(J - 1)^2, \quad (4)$$

that serves as a penalty function enforcing the compressibility constraint. The parameters  $c$  and  $k_1$  are the material parameters (stress coefficients) and  $k_2$  is a dimensionless material parameter. The invariants were defined as  $\bar{I}_1$  and  $\bar{I}^*$  and  $J$  is the local volume ratio (Holzapfel, 2002). The strain energy potentials in the Prosthesis model is defined as Eq. (5),

$$U = C10(I_1 - 3) + C01(I_2 - 3) + \frac{1}{D_1}(J - 1)^2, \quad (5)$$

where  $U$  is the strain energy,  $C10$  and  $C01$  are material constants,  $\bar{I}_1$  and  $\bar{I}_2$  are deviatoric strain invariants. The  $D_1$  is defined as Eq. (6) (Iatridis et al., 1996)

$$D_1 = \frac{3(1 - 2V)}{\mu(1 + \nu)}, \quad (6)$$

where  $\mu$  is the shear modulus and  $\nu$  is the Poisson's ratio.

## 2.2.2 Intradiscal Parameters Estimation:

The intradiscal parameters including the pressure were calculated at the mid-plane of the disc. The pressure value's sign refer to the direction where negative and positive pressure values refer to the extension and tension, respectively. The Intradiscal pressure is the distribution of load across the end plate of the disc toward center, as the hydrostatic pressure in nucleus (Noailly et al., 2005).

## 3. Results and Discussion

The ultimate goal of the current study is to statically assess the three-dimensional geometry of the L3-L5 lumbar spine using a finite element method coupled with the fibre-reinforced constitutive formulation introduced by Holzapfel (Holzapfel & Stadler, 2006). The simulations were performed in two stages of intact lumbar spine (INT model) included natural intervertebral discs between L3, L4 and L5 and a L3-L5 lumbar spine with an implanted CAdisc between L4 and L5 (IMP).

### 3.1 Computing the Complete Intersegmental Rotation in Flexion

#### 3.1.1 The Intersegmental Rotation of Natural Disc Between L3 and L4

As shown in Fig. 2, the modeling results predicted a 4% increase in intersegmental rotation of L3-L4 when the SSL was removed. Noailly et al. (2007) reported 0.8% of increase for their rough model and 1.2% increase for their updated model.

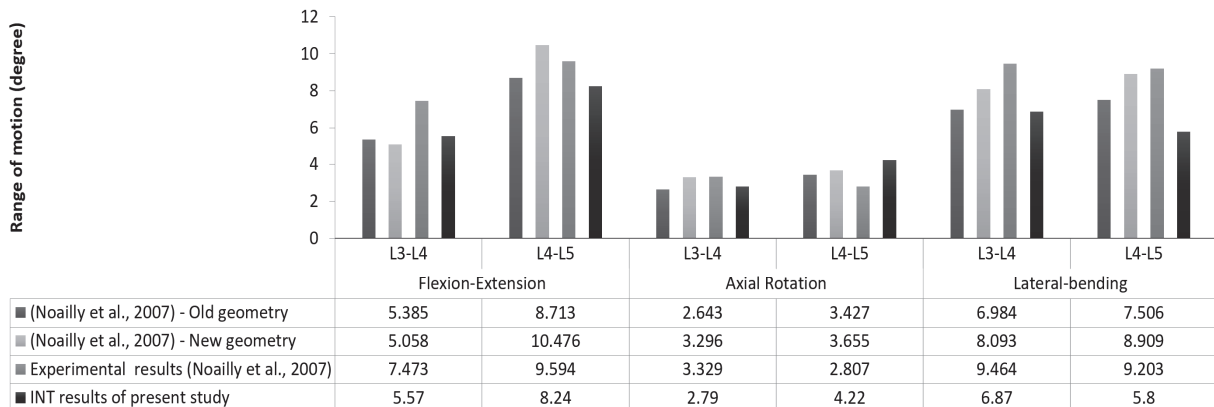


**Fig. 2.** Ranges of motions in sagittal flexion at 7.5Nm; absolute values for the intact version of each geometry and after each component resection. A glossary of the abbreviations is given in Table 1.

By removing the CL, our model predicted 84% increase in the intersegmental rotation of L3-L4 segment that was similar to the reported data from the rough model of Noailly et al. (2007), 84% predicted increase by our model against their updated model predicted 146% increase. Finally, by removing the ITL, the intersegmental rotation of L3-L4 segment estimated by our INT model increased by 0.2%, while this value was reported as 1% and 2% for the rough and updated models by Noailly et al (2007).

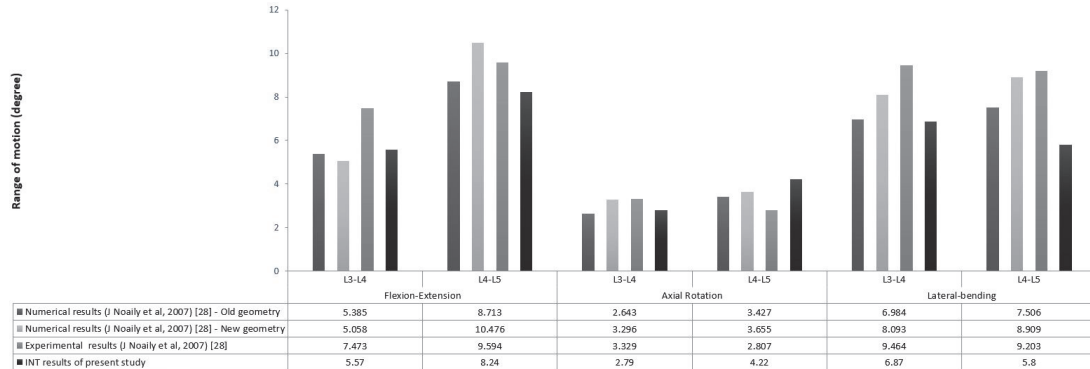
#### 3.1.2 The Intersegmental Rotation of Natural Disc between L4 and L5

Fig. 2 shows 2% increase in intersegmental rotation of L4-L5 after removing the SLL calculated by the presented INT model while Noailly et al. (2007) reported no increase using the rough and the updated models. By removing the FLL, the intersegmental rotation of L4-L5 segment shown a 0.4% increase using the same INT model while this value was reported 4% and 0% for the rough and updated models of Noailly et al. (2007). The same parameter after the CL was removed was estimated to be 36% compared the reported data of 36% and 30% for the rough and updated models of Noailly et al. (2007).

### 3.2 Computing the Range of Motion of FEM Intact Model

#### 3.2.1 The range of motion in flexion-extension

Fig. 3 depicts that in flexion-extension, the range of motion of L3-L4 segment using the presented INT model was 25% lower than the experimental data reported by Noailly et al. (2007). Furthermore, this parameter for the L4-L5 was estimated to be 14% lower than the experimental results of Noailly et al. (2007).



**Fig. 3.** Comparison of the computed ranges of motion given by our intact models with experimental and numerical results of similar previous studies for 7.5Nm pure moments.

#### 3.2.2 The Range of Motion in Axial-Rotation

The range of motion of L3-L4 segment in axial rotation calculated by the INT model was estimated to be 27% lower than the experimental data in the literature (Noailly et al., 2007), Fig. 3. The same parameter for the L4-L5 segment was shown to be 37% less than the literature reported data (Noailly et al., 2007).

#### 3.2.3 The Range of Motion in Lateral Bending

The lateral bending range of motion values of L3-L4 and L4-L5 were estimated by the INT model to be 16% and 50% lower than the reported data in the literature (Noailly et al., 2007), respectively, Fig. 3.

### 3.3 Computing the Range of Motion of FEM Model of Cadisc-L (IMP)

Table 3 summarizes the range of motion values at different conditions comparing the IMP and INT models. In term of flexion-extension, the range of motion for the L3-L4 when IMP model was used was shown to be 1.7% larger than the results of the INT model while this value was shown to be 50% lower compared to INT model.

**Table 3.** Comparison of the computed ranges of motion between our intact model (INT) and the model with the L4-L5 Cadisc (IMP) for 7.5Nm pure moments.

Range of motion (degrees)		INT model	IMP model	Difference of INT to IMP (%)
Flexion-Extension	L3-L4	5.57	5.67	-1.79
	L4-L5	8.24	4.58	44.41
Axial Rotation	L3-L4	2.79	2.74	1.79
	L4-L5	4.22	4.44	-5.21
Lateral-bending	L3-L4	6.87	6.87	0
	L4-L5	5.8	3.86	33.44

In term of axial rotation, the L3-L4 range of motion estimated to be 1.8% lower when IMP model was used to compare to the INT. However, the same parameter for the L4-L5 case was shown to be 5% larger when IMP model was used to compare to the INT model.

### 3.3.3 The range of motion in lateral bending

Considering the lateral bending, the L3-L4 range of motion estimation using IMP model was shown to be 0.01% lower than INT model while this value for the L4-L5 case was 33%.

### 3.4 Intradiscal Pressure

Fig. 4 and Fig. 5 show the intradiscal pressure changes. The peak of intradiscal pressure for the L3-L4 predicted by the IMP model was 0.4 MPa. The same parameter for the L4-L5, when the IMP model was used, was reported lower than those reported by the INT model from relative distance of 0 to 18 mm. The peak intradiscal pressure of L4-L5 segment was shown to be 0.6 MPa.

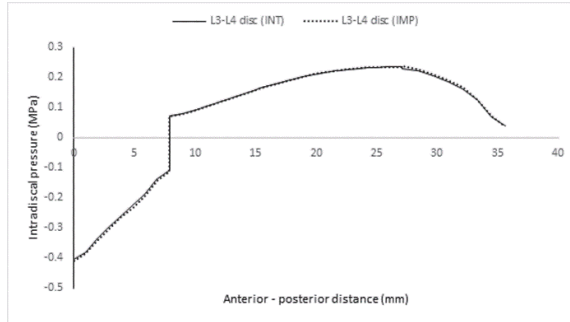


**Fig. 4.** Intradiscal pressure of L3-L4 along an anterior-posterior mid-sagittal path for 7.5Nm pure moments. Note the INT refers to our intact model and IMP refers to the model with the L4-L5 Cadisc

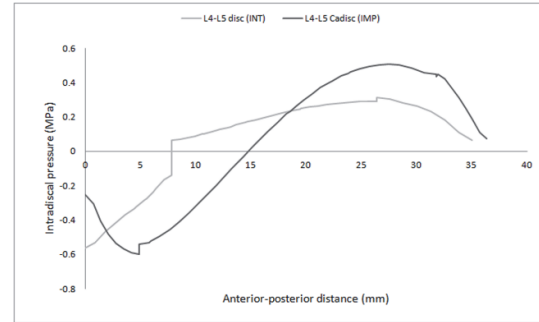


**Fig. 5.** Intradiscal pressure of L4-L5 along an anterior-posterior mid-sagittal path for 7.5Nm pure moments. Note the INT refers to our intact model and IMP refers to the model with the L4-L5 Cadisc

### 3.5 Intradiscal Von-Mises Stress

#### 3.5.1 Intradiscal von-Mises stress of L3-L4 along an anterior-posterior mid-sagittal path

The intradiscal Von-Mises stress changes of L3-L4 segment in flexion is demonstrated in Fig. 6 with a peak of 0.8 MPa using the IMP model.

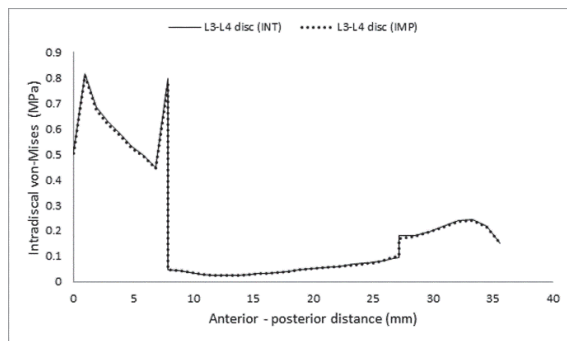


**Fig. 6.** Intradiscal von-Mises stress of L3-L4 along an anterior-posterior mid-sagittal path for 7.5Nm pure moments. Note the INT refers to our intact model and IMP refers to the model with the L4-L5 Cadisc

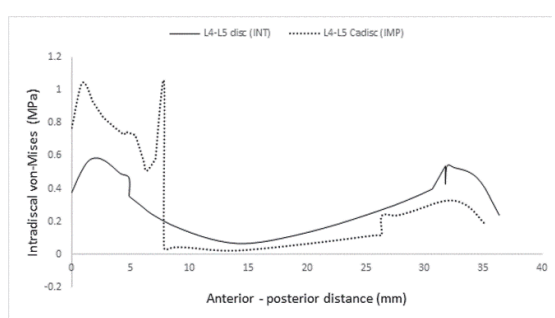


**Fig. 7.** Intradiscal von-Mises stress of L4-L5 along an anterior-posterior mid-sagittal path for 7.5Nm pure moments. Note the INT refers to our intact model and IMP refers to the model with the L4-L5 Cadisc

Fig. 7 shows the L4-L5 intradiscal Von-Mises stress changes in flexion using the IMP model at a relative distance of 0 to 8 mm with a peak at 0.6 MPa.

This comparison of the reported INT modeling data of the current paper with those reported in the literature under similar loading conditions at the healthy state are shown to be in a reasonable agreement. The validated model was further used to include the Cadisc-L in the L4-L5 position to evaluate its mechanical behavior. To describe the composition of Cadisc-L and its biophysical

properties, Gwynne and Cameron (2010) applied small angle X-ray scattering to examine the variation in annulus and nucleus domains segregated by a graduated region. This experiment also included the calculation of intensity ratios. Moreover, a linescan technique was used to determine the change. Van den Broek et al., (2012) is in good agreement with our findings, although they did not include Ca-disc mechanical properties. Van den Broek et al. (2012) concluded that mimicking the intervertebral disk's non-linear behavior is essential in supporting the spinal motion. As shown in Fig. 2, the largest impact of the different ligamentous resections of spine was achieved after CL elimination. This estimation is in good agreement with the literature (Adams et al., 1980; Twomey & Taylor, 1983; Noailly et al., 2005; 2007). Furthermore, the largest effect of different ligamentous resections of spine at intersegmental rotation of natural disc was observed for L4-L5 (Fig. 2). This prediction is mostly in agreement with reported studies (Noailly et al., 2005; 2007). Our FEM-predicted results of INT model are in agreement with Noailly et al.'s findings (Noailly et al., 2005, 2007) for 'range of motion' (Fig. 3 and Table 3). It appears that the observed differences might be due to geometrical differences. It should be mentioned that such differences were observed by Noailly et al. when they compared their numerical and experimental models (Noailly et al., 2005; 2007). To the best of the authors' knowledge, there is no comparable study in the literature that predicts the mechanical behavior of the IMP model.

#### 4.3 Cadisc-L implantation

A negligible (less than 1.8%) difference in the results for the range of motion of L3-L4 was observed when both models were used, as shown in Table 3. The FEM-predicted intradiscal pressure and von-Mises stress of L3-L4 along a straight path in an anterior-posterior direction, belonging to the mid-sagittal plane, shows qualitative agreement between our FEM-predicted results of IMP and INT models (Figs. 4 and 6). The range of motion of L4-L5 intervertebral CADisc in IMP model was reduced by 50% in flexion-extension and 33% in lateral-bending (Table 3). This demonstrates that the range of motion is less affected due to implantation of Cadisc as compared to other artificial discs (McNally et al., 2012). The FEM-predicted intradiscal pressure and von-Mises stress of L4-L5 along a straight path in an anterior-posterior direction, belonging to the mid-sagittal plane, shows good agreement between Our FEM-predicted results of IMP and INT models (Figs. 5 and 7).

#### 4.4 Limitations and future trends

The current study was performed statically while it's naturally a dynamic process. A comprehensive dynamic study may produce better results for future studies. Since the developed model in this study is not a parametric one, it is challenging to change the dimensions of the geometry in a short time. Developing a parametric model in the future will enable researchers to study the size variation effects.

The Holzapfel method is neo-Hookean equation-base (Holzapfel & Stadler, 2006) that was available in the commercial CFD package, Abaqus. We suggest the Mooney-Rivlin equation in future studies in order to be comparable to other studies of similar material properties. The advantage of Holzapfel method is that it requires less solution time. It should be highlighted that facet joint orientations may have great influence on interaction in each model and make the mechanical behavior different. Therefore, more real conclusions can be extracted by considering more real geometry in future studies.

Isotropic mechanical properties were considered for the annulus for the sake of simplicity while it's an anisotropic that can be investigated in the future studies. We are proposing to apply the adjacent level prediction data when the stiff prostheses are in use in segments loaded using different protocols, considering fibre-reinforced constitutive formulation introduced by Holzapfel and Stadler (Holzapfel & Stadler, 2006).

### 5. Conclusion

A three-dimensional finite element model of lumbar vertebrate is developed comprising L3, L4 and L5 to predict the mechanical behavior of a natural and Cadisc. The fibre-reinforced constitutive

formulation introduced by Holzapfel (Holzapfel & Stadler, 2006) was applied. This has the merit of requiring only a single scalar structure parameter to specify the dispersion of the fibres. The relatively quick solution time was achieved using the three-dimensional model with the parametric method introduced by Holzapfel (Holzapfel & Stadler, 2006). The model developed was used to make predictions of inter-segmental rotations and range of motions in flexion-extension, axial rotation, and lateral bending in natural and artificial discs. The modeling data in the IMP case revealed that the range of motion for the Cadisc implant decreased by 50% in flexion and 33% in lateral bending as compared to the intact case.

## References

- Adams, M. A., Hutton, W. C., & Stott, J. R. (1980). The resistance to flexion of the lumbar intervertebral joint. *Spine*, 5(3), 245-253.
- Amerian, M., Bahraseman, H. G., Leilnahari, K., Khodaloffi, M., Amerian, M., & Bahmani, A. (2014). Modeling of the Effect of Backpack Load Position on the Lumbar Spine Curvature. *Annual Research & Review in Biology*, 4(4), 638.
- Bahraseman, H. G., Hassani, K., Navidbakhsh, M., Espino, D. M., Kazemi-Saleh, D., & Fatourayee, N. (2013). Estimation of maximum intraventricular pressure: A three-dimensional fluid-structure interaction model. *Biomedical engineering online*, 12(1), 122.
- Bahraseman, H. G., Hassani, K., Khosravi, A., Navidbakhsh, M., Espino, D. M., Fatouraee, N., & Kazemi-Saleh, D. (2014a). Combining numerical and clinical methods to assess aortic valve hemodynamics during exercise. *Perfusion*, 29(4), 340-350.
- Bahraseman, H. G., Hassani, K., Navidbakhsh, M., Espino, D. M., Sani, Z. A., & Fatouraee, N. (2014b). Effect of exercise on blood flow through the aortic valve: a combined clinical and numerical study. *Computer Methods in Biomechanics and Biomedical Engineering*, 17(16), 1821-1834.
- Bahraseman, H., Hamzehei, B., Leilnahari, K., Khosravi, A., & Languri, E. (2015). Experimental and computational study on the effects of wearing neck collar on the carotid blood flow. *Engineering Solid Mechanics*, 3(1), 27-34.
- Bahraseman, H. G., Languri, E. M., Yahyapourjalaly, N., & Espino, D. M. (2016). Fluid-Structure Interaction modeling of aortic valve stenosis at different heart rates. *Acta of Bioengineering and Biomechanics*, 18(3).
- Barnes, D., Johnson, S., Snell, R., & Best, S. (2012). Using scratch testing to measure the adhesion strength of calcium phosphate coatings applied to poly (carbonate urethane) substrates. *Journal of the Mechanical Behavior of Biomedical Materials*, 6, 128-138.
- Benzel, E. C., Lieberman, I. H., Ross, E. R., Linovitz, R. J., Kuras, J., & Zimmers, K. (2011). Mechanical characterization of a viscoelastic disc for lumbar total disc replacement. *Journal of Medical Devices*, 5(1), 011005.
- Berkson, M. H., Nachemson, A., & Schultz, A. (1979). Mechanical properties of human lumbar spine motion segments—part II: responses in compression and shear; influence of gross morphology. *Journal of Biomechanical Engineering*, 101(1), 53-57.
- Brown, T., Hansen, R. J., & Yorra, A. J. (1957). Some mechanical tests on the lumbosacral spine with particular reference to the intervertebral discs: a preliminary report. *JBJS*, 39(5), 1135-1164.
- Chen, S. H., Zhong, Z. C., Chen, C. S., Chen, W. J., & Hung, C. (2009). Biomechanical comparison between lumbar disc arthroplasty and fusion. *Medical Engineering & Physics*, 31(2), 244-253.
- Chen, C. S., Cheng, C. K., Liu, C. L., & Lo, W. H. (2001). Stress analysis of the disc adjacent to interbody fusion in lumbar spine. *Medical Engineering & Physics*, 23(7), 485-493.
- Denoziere, G. (2004). *Numerical modeling of a ligamentous lumbar motion segment* (Doctoral dissertation, Georgia Institute of Technology).
- Dietrich, M., Kedzior, K., Borkowski, P., NSKI, G. K., Skalski, K., & Zagajek, T. (2005). A nonlinear analysis of the human vertebral column and medical recommendations that follow. *TECHNICAL SCIENCES*, 53(3).

- Dietrich, M., Kedzior, K., & Zagrajek, T. (1991). A biomechanical model of the human spinal system. *Proceedings of the Institution of Mechanical Engineers, Part H: Journal of Engineering in Medicine*, 205(1), 19-26.
- Eberlein, R. O. B. E. R. T., Holzapfel, G. A., & Schulze-bauer, C. A. (2001). An anisotropic model for annulus tissue and enhanced finite element analyses of intact lumbar disc bodies. *Computer Methods in Biomechanics and Biomedical Engineering*, 4(3), 209-229.
- Falodi, A. (2010). *Prediction of the biomechanical performance of a novel total disc replacement* (Doctoral dissertation, University of Nottingham).
- Gloria, A., De Santis, R., Ambrosio, L., Causa, F., & Tanner, K. E. (2011). A multi-component fiber-reinforced PHEMA-based hydrogel/HAPEXTM device for customized intervertebral disc prosthesis. *Journal of Biomaterials Applications*, 25(8), 795-810.
- Goel, V. K., Fromknecht, S. J., Nishiyama, K., Weinstein, J., & Liu, Y. K. (1985). The role of lumbar spinal elements in flexion. *Spine*, 10(6), 516-523.
- Goel, V. K., Monroe, B. T., Gilbertson, L. G., & Brinckmann, P. (1995). Interlaminar shear stresses and laminae separation in a disc: finite element analysis of the L3-L4 motion segment subjected to axial compressive loads. *Spine*, 20(6), 689-698.
- Gwynne, J. H., Oyen, M. L., & Cameron, R. E. (2010). Preparation of polymeric samples containing a graduated modulus region and development of nanoindentation linescan techniques. *Polymer Testing*, 29(4), 494-502.
- Gwynne, J. H., & Cameron, R. E. (2010). Using small angle X-ray scattering to investigate the variation in composition across a graduated region within an intervertebral disc prosthesis. *Journal of Materials Science: Materials in Medicine*, 21(2), 787-795.
- Holzapfel, G. A. (2002). Nonlinear solid mechanics: a continuum approach for engineering science. *Meccanica*, 37(4), 489-490.
- Holzapfel, G. A., & Stadler, M. (2006). Role of facet curvature for accurate vertebral facet load analysis. *European Spine Journal*, 15(6), 849-856.
- Iatridis, J. C., Weidenbaum, M., Setton, L. A., & Mow, V. C. (1996). Is the nucleus pulposus a solid or a fluid? Mechanical behaviors of the nucleus pulposus of the human intervertebral disc. *Spine*, 21(10), 1174-1184.
- Johnson, S., Naylor, J., & McNally, D. (2011). In vitro biomechanical comparison of the native intervertebral disc and a compliant artificial lumbar disc replacement (Cadisc-L). *The Spine Journal*, 11(10), S153.
- Joshi, A., Fussell, G., Thomas, J., Hsuan, A., Lowman, A., Karduna, A., ... & Marcolongo, M. (2006). Functional compressive mechanics of a PVA/PVP nucleus pulposus replacement. *Biomaterials*, 27(2), 176-184.
- Kędzior, K., Krzesiński, G., & Zagrajek, T. (1996). Numerical simulation of the scoliosis as caused by mechanical response of the spinal segment to external load. In *Lecture Notes of the Intern. Centre of Biocybernetics Seminars* (Vol. 33, pp. 158-164).
- Khosravi, A., Bahraseman, H., Hassani, K., & Kazemi-Saleh, D. (2014a). Numerical method to measure velocity integration, stroke volume and cardiac output while rest: using 2D fluid-solid interaction model. *Engineering Solid Mechanics*, 2(2), 91-100.
- Khosravi, A., Bahraseman, H. G., Saleh, A. V., & Kazemi-Saleh, D. (2014b). Initial insight to effect of exercise on maximum pressure in the left ventricle using 2D fluid-structure interaction model. *Annual Research & Review in Biology*, 4(18), 2867.
- Langrana, N. A., Lee, C. K., & Yang, S. W. (1991). Finite-element modeling of the synthetic intervertebral disc. *Spine*, 16(6 Suppl), S245-52.
- Leilnahari, K., Bahraseman, H. G., & Sadeghy, M. (2013). Assessment of an arm-positioning pillow to prevent waking paresthesia symptoms related to side sleepers: using echo-Doppler imaging.
- Logan, D.L., A first course in the finite element method. 2nd ed. 1992, Boston: PWS-Kent Pub. Co. xx, 662 p.

- McNally, D., Naylor, J., & Johnson, S. (2012). An in vitro biomechanical comparison of Cadisc™-L with natural lumbar discs in axial compression and sagittal flexion. *European Spine Journal*, 21(5), 612-617.
- Miller, J. A. A., Schultz, A. B., Warwick, D. N., & Spencer, D. L. (1986). Mechanical properties of lumbar spine motion segments under large loads. *Journal of Biomechanics*, 19(1), 79-84.
- Nachemson, A. L., Schultz, A. B., & Berkson, M. H. (1979). Mechanical properties of human lumbar spine motion segments. Influence of age, sex, disc level, and degeneration. *Spine*, 4(1), 1-8.
- Natarajan, R. N., & Andersson, G. B. (1999). The influence of lumbar disc height and cross-sectional area on the mechanical response of the disc to physiologic loading. *Spine*, 24(18), 1873.
- Noailly, J., Ambrosio, L., Tanner, K. E., Planell, J. A., & Lacroix, D. (2012). In silico evaluation of a new composite disc substitute with a L3-L5 lumbar spine finite element model. *European Spine Journal*, 21(5), 675-687.
- Noailly, J., Lacroix, D., & Planell, J. A. (2005). Finite element study of a novel intervertebral disc substitute. *Spine*, 30(20), 2257-2264.
- Noailly, J., Wilke, H. J., Planell, J. A., & Lacroix, D. (2007). How does the geometry affect the internal biomechanics of a lumbar spine bi-segment finite element model? Consequences on the validation process. *Journal of Biomechanics*, 40(11), 2414-2425.
- Polikeit, A., Ferguson, S. J., Nolte, L. P., & Orr, T. E. (2003). Factors influencing stresses in the lumbar spine after the insertion of intervertebral cages: finite element analysis. *European Spine Journal*, 12(4), 413-420.
- Poor, M. G., Bahraseman, H. G., Pouranbarani, E., Sarang, R., Shafieian, M., & Leilnahari, K. (2017). A Comparative Study in Cervical Muscle Activities during Various Resting Postures Using Electromyography. *American Journal of Biomedical Sciences*, 9(3).
- Rohlmann, A., Zander, T., Schmidt, H., Wilke, H. J., & Bergmann, G. (2006). Analysis of the influence of disc degeneration on the mechanical behaviour of a lumbar motion segment using the finite element method. *Journal of Biomechanics*, 39(13), 2484-2490.
- Sabooni, H., Hassani, K., & Bahraseman, H. G. (2015). Modeling of iliac artery aneurysm using fluid-structure interaction. *Journal of Mechanics in Medicine and Biology*, 15(01), 1550041.
- Schultz, A. B., Warwick, D. N., Berkson, M. H., & Nachemson, A. L. (1979). Mechanical properties of human lumbar spine motion segments—Part I: responses in flexion, extension, lateral bending, and torsion. *Journal of Biomechanical Engineering*, 101(1), 46-52.
- Shin, D. S., Lee, K., & Kim, D. (2007). Biomechanical study of lumbar spine with dynamic stabilization device using finite element method. *Computer-Aided Design*, 39(7), 559-567.
- Shirazi-Adl, A. A. A. S. S., Ahmed, A. M., & Srivastava, S. C. (1986). Mechanical response of a lumbar motion segment in axial torque alone and combined with compression. *Spine*, 11(9), 914-927.
- Skalli, W. (1999). Spine biomechanics. From basic research to clinical applications. *Acta of Bioengineering and Biomechanics*, 1(Suppl 1), 379-384.
- Tencer, A. F., Ahmed, A. M., & Burke, D. L. (1982). Some static mechanical properties of the lumbar intervertebral joint, intact and injured. *Journal of Biomechanical Engineering*, 104(3), 193-201.
- Twomey, L. T., & Taylor, J. R. (1983). Sagittal movements of the human lumbar vertebral column: a quantitative study of the role of the posterior vertebral elements. *Archives of Physical Medicine and Rehabilitation*, 64(7), 322-325.
- Van den Broek, P. R., Huyghe, J. M., Wilson, W., & Ito, K. (2012). Design of next generation total disk replacements. *Journal of Biomechanics*, 45(1), 134-140.
- Zienkiewicz, O.C., & Taylor, R.L (1991). *The Finite Element Method*. McGraw-Hill, London.



© 2018 by the authors; licensee Growing Science, Canada. This is an open access article distributed under the terms and conditions of the Creative Commons Attribution (CC-BY) license (<http://creativecommons.org/licenses/by/4.0/>).